

## Article

# Research on Ultraviolet Characteristic Parameters of DC-Positive Polarity Corona Discharge on Conductors

Youquan Dai <sup>1</sup>, Zhanlong Zhang <sup>1,\*</sup>, Zijian Dong <sup>1</sup>, Yongye Wu <sup>1,2</sup> and Deng Jun <sup>1</sup>

<sup>1</sup> School of Electrical Engineering, Chongqing University, Chongqing 400044, China; 20173445@cqu.edu.cn (Y.D.); dongzj@cqu.edu.cn (Z.D.); wuyongye@alu.cqu.edu.cn (Y.W.); 202311131125t@stu.cqu.edu.cn (D.J.)

<sup>2</sup> Chengdu Power Supply Company, Chengdu 610002, China

\* Correspondence: zhangzl@cqu.edu.cn

**Abstract:** The detection of corona-related defects in transmission lines has been included in the work of transmission line defect detection. Ultraviolet detection technology has gradually been widely applied in the field of corona discharge detection. However, the current research on the application of ultraviolet detection technology in transmission lines is relatively simple and mainly limited to using changes in the photon count to determine whether corona discharge has occurred. To address this, this study used a mini corona cage to simulate transmission lines and measured the changes in the photon count, spot area, and corona current in the corona inception process of different types of smooth, stainless-steel conductors. This study also investigated the variations in the photon count and spot area depending on conductor corona intensity, ultraviolet imager gain, and observation distance. The results show that the photon count and spot area can, to some extent, reflect the intensity of corona discharge. Both the photon count and spot area exhibited quadratic relationships with the voltage. As the observation distance increased, both the photon count and spot area showed exponential decay. The photon count exhibited a trend of initially increasing, then decreasing, and finally increasing again with the increase of gain, while the spot area showed exponential growth with increasing gain. The photon count and spot area can complement each other to identify and characterize the intensity of corona discharge.

check for  
updates

**Citation:** Dai, Y.; Zhang, Z.; Dong, Z.; Wu, Y.; Jun, D. Research on Ultraviolet Characteristic Parameters of DC-Positive Polarity Corona Discharge on Conductors. *Appl. Sci.* **2024**, *14*, 3258. <https://doi.org/10.3390/app14083258>

Academic Editor: Roberto Zivieri

Received: 27 February 2024

Revised: 9 April 2024

Accepted: 10 April 2024

Published: 12 April 2024



**Copyright:** © 2024 by the authors. Licensee MDPI, Basel, Switzerland. This article is an open access article distributed under the terms and conditions of the Creative Commons Attribution (CC BY) license (<https://creativecommons.org/licenses/by/4.0/>).

**Keywords:** corona discharge; UV imaging; photon number; gain; observation distance

## 1. Introduction

The adoption of ultra-high-voltage (UHV) transmission is becoming an inevitable trend in the development of power grids. Electromagnetic environmental issues stemming from corona discharge on transmission lines are significant technical concerns that must be carefully considered during the design, construction, and operation of UHV transmission lines [1–3]. The detection of corona-related defects in transmission lines has been included in the scope of defect detection work for transmission lines. In recent years, ultraviolet (UV) detection technology has been widely applied for the accurate, fast, visual, and safe detection of corona discharges in electrical equipment [4–9]. Some relevant studies [10–13] have been conducted on the corona inception voltage of conductors using ultraviolet detection technology. Some studies have used ultraviolet image processing techniques to quantify the situation of corona discharge [14,15]. The ultraviolet imaging instrument primarily reflects the intensity of corona discharge through the number of ultraviolet photons and the size of the light spot, and the measurement results are significantly affected by the settings of the observation distance and gain. Currently, the research on the variations in the photon count and spot area depending on the corona discharge intensity, as well as the observation distance and gain of the ultraviolet imaging system, is primarily focused on applications related to insulators [16] and needle-plane discharge

models [17]. Therefore, it is necessary to study the variations in the photon count and light spot area depending on conductor voltage, as well as the gain and observation distance settings of the ultraviolet imaging system, to provide references for the detection of corona discharge on transmission lines using ultraviolet imaging instruments. Studying the corona discharge process of conductors using a corona cage is closer to the actual conditions of power transmission lines and offers advantages, such as low cost, controllable experimental conditions, convenient structural adjustments, ease of measurement, and shorter experimental cycles [18–20]. Therefore, utilizing a corona cage in the laboratory to investigate the variations in the photon count and light spot area with conductor voltage, as well as changes in the gain and observation distance of the ultraviolet imaging system, represents an effective experimental approach. This study utilized a mini corona cage to measure the variations in photon count, spot area, and corona current during the corona inception process of different types of smooth, stainless-steel conductors. The functions relating the ultraviolet photon count and spot area to conductor voltage for different conductors were obtained through fitting using the least squares method. The fitting results indicate that both the ultraviolet photon count and spot area exhibited a quadratic relationship with the conductor voltage. Additionally, this study investigated the variations in the photon count and spot area with respect to the gain and observation distance of the ultraviolet imaging system and performed relevant function fittings to capture these relationships. The spot area data obtained at different gains and observation distances were integrated to reference gains and spot areas. By combining the fitting functions of the photon count and spot area with respect to the conductor voltage at the reference gain and reference observation distance, the measured ultraviolet photon count or measured spot area can be used to estimate the corresponding conductor voltage, facilitating the assessment of the discharge severity. The above-mentioned research provides valuable application references for utilizing ultraviolet imaging to assess corona discharges in power transmission lines.

## 2. Construction of Experimental Platform and Experimental Methods

The experimental environment is characterized by a temperature of approximately 15 °C, a relative humidity of around 75%, and an atmospheric pressure of 101.5 kPa. In this study, mini corona cages were selected to simulate transmission lines. The corona cage structure employed a commonly used steel framework and metal mesh configuration. To ensure a uniform distribution of the electric field intensity on the conductor surface during measurements and to avoid end effects, the corona cage was divided into three sections. The total length of the corona cage was 1 m, with the middle section measuring 50 cm and both sides measuring 25 cm each. The diameter of the cage was 30 cm. As shown in Figure 1, the middle section served as the measurement segment, which uniformly surrounded the conductor. The two ends were directly grounded as protective segments to weaken the end effects and were not used for measurements. The measurement segment in the middle and the protective sections on both sides were insulated through an air gap. In the experiment, the conductors were placed in the center of the corona cage using insulating supports. Following the methods recommended by the International Council on Large Electric Systems (CIGRE) and the International Special Committee on Radio Interference (CISPR), the actual operating split conductor is first equivalent to a single conductor, and then the conductor radius is reduced proportionally to allow it to corona at a lower voltage. In the experiment, smooth, stainless-steel rods with diameters of 2 mm, 3 mm, and 5 mm were used to simulate actual transmission lines. The main equipment included in the experimental setup consisted of a DC high-voltage generator, which was used to generate the required high voltage for the experiment. In this experiment, the model of the high-voltage generator used was JYDHV-100 kV/3 mA. It has an adjustable output DC voltage range of 0 to 100 kV, with a maximum protection current of 3 mA. One ammeter was used to measure the current on the conductor, which has a measurement range of 0 to 2 mA. During the experiment, the STUV-11 ultraviolet imaging camera, which is a day-blind type, was positioned directly facing the discharge location.

Only the instrument gain and observation distance were varied, while the other parameters were kept at their default settings. During the experiment, an ultraviolet imaging camera and ammeters were used to measure the UV image and corona current, respectively, to reflect the changes in the severity of the corona discharge depending on the voltage applied to the conductor and the observation distance and gain of the UV imaging device.

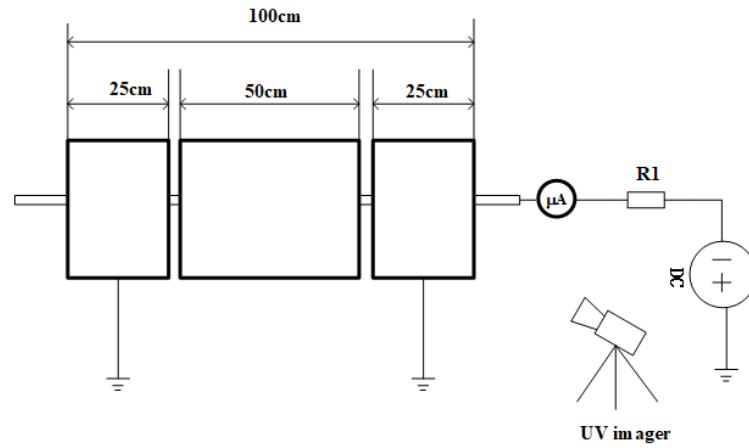


Figure 1. Schematic diagram of experimental platform.

STUV-11 UV imagers were used in the experiments, as shown in Figure 2. The basic parameters of the UV imagers are shown in Table 1.



Figure 2. Ultraviolet (UV) imagers.

Table 1. Basic parameters of the ultraviolet (UV) imager.

TYPE	Sensitivity (W/cm <sup>2</sup> )	Detection Distance (m)	Range of Imager Gain
STUV-11	$1.8 \times 10^{-18}$	0.5~100	0~100

Under the influence of DC voltage, the dispersion of the DC breakdown voltage in air gaps is generally minimal. The equation for estimating the corona inception field strength for positive polarity conductors can be approximated using the empirical formula proposed by J.B. Whitehead, as shown in Equation (1) [21].

$$E_{on+} = 33.7m\delta\left(1 + \frac{0.24}{\sqrt{r_0\delta}}\right) \tag{1}$$

In the equation,  $E_{on+}$  represents the corona inception field strength for positive polarity, and  $\delta$  is the relative density of air,  $\delta = 0.00289p / (273 + \theta)$ .  $p$  is the atmospheric pressure in pascals (Pa),  $\theta$  is the temperature in degrees Celsius (°C), and  $m$  is the roughness factor for smooth conductors; as used in this study, the roughness factor can be taken as 1.

For the coaxial cylindrical electrode structure used in this study, the relationship between the corona inception field strength and the corona inception voltage can be expressed

as Equation (2). By combining Equations (1) and (2), the corona inception voltage for the selected conductor in the mini corona cage can be determined.

$$E_{on} = \frac{U_{on}}{r_0 \ln(r_R/r_0)} \quad (2)$$

In the equation,  $E_{on}$  represents the nominal surface electric field strength on the conductor (kV/cm),  $U_{on}$  represents the voltage applied between the conductor and the corona cage (kV),  $r_0$  represents the radius of the conductor (cm), and  $r_R$  represents the radius of the corona cage (cm).

For a certain diameter of the conductor, the diameter of the corona cage needs to be sufficiently small so that the conductor can exhibit the corona phenomenon at lower voltages. Additionally, there should be a sufficient air gap between the conductor and the cage walls to ensure that the breakdown voltage is at least 50% higher than the corona inception voltage. This design ensures stable observation and analysis of the corona phenomenon [22].

By combining Equations (1) and (2), it can be determined that the corona voltage range of the conductor selected in this paper was 28~51 kV under the selected corona cage size. According to the calculation based on the breakdown voltage of the easiest-to-inception positive rod-negative plate gap, the average breakdown field strength was approximately 5 kV/cm. Therefore, the breakdown voltage for a 15 cm gap was estimated as 75 kV. The calculation results indicate that the breakdown voltage was 47% higher than the corona inception voltage. Therefore, the corona cage structure used in this study essentially meets the requirements for corona inception voltage and breakdown voltage.

Based on the analysis provided above, it can be concluded that the corona cage and conductor used in the experiment meet the experimental requirements. Within the applied voltage range, the corona cage allowed the conductor to initiate corona discharge effectively while providing a certain margin to observe the phenomenon without reaching the breakdown voltage. As the applied voltage on the conductor increased, the surface electric field strength of the conductor gradually exceeded the corona inception electric field, and corona discharge began. During the experimental process, before the conductor started to corona, the surface electric field of the conductor was proportional to the voltage, increasing with the increase in voltage and decreasing with the increase in the conductor radius. After the conductor started to corona, the electric field near the conductor was the composite value of the nominal electric field of the conductor and the spatial charge electric field generated by the corona discharge. However, overall, the electric field near the conductor is positively correlated with the voltage and negatively correlated with the conductor radius [23].

### 3. Results and Analysis of Ultraviolet Photon Counting

#### 3.1. Variation Characteristics of Photon Count Based on Discharge Intensity

This study examined the corona inception process of the conductor from two aspects: ultraviolet photon counting and corona current measurement. Based on the experimental measurements, the corona current and ultraviolet photon count results of the smooth conductor at different voltages were obtained. The inflection point method was utilized to determine the corona inception voltage of the conductor [24]. By gradually applying voltage to the conductor, the discharge process went through a progression from corona inception to full corona discharge. During this process, the ultraviolet photon count and corona current increased correspondingly. The experimental procedure adopted during the experiment was as follows:

- (1) Voltage was applied to the conductor and slowly increased until corona discharge was observed. The voltage was maintained at a constant level once corona discharge was established for observation and data collection purposes. After that, we started recording the ultraviolet detection data while simultaneously using the ammeter to measure the corona current. To avoid errors caused by random data, the voltage was

- kept constant. The average readings of the ultraviolet imager and the ammeter within 10 s were recorded as the measurement results, and then the voltage was slowly increased. The above detection process was repeated for each voltage increment.
- (2) Based on the controlled variable method, the gain and observation distance of the ultraviolet imaging camera were varied. The ultraviolet imaging camera was used to detect the change in the photon count around the conductor inside the corona cage. To avoid the influence of occasional data, the average value of the ultraviolet photon count measured over 10 s was taken as the measurement result.
  - (3) After concluding the experiment, we waited for a certain period until the space charge had fully dissipated. Then, we replaced the conductor and repeated the aforementioned steps.

Several typical ultraviolet images captured during the corona inception process of the 5 mm conductor are shown in Figure 3.

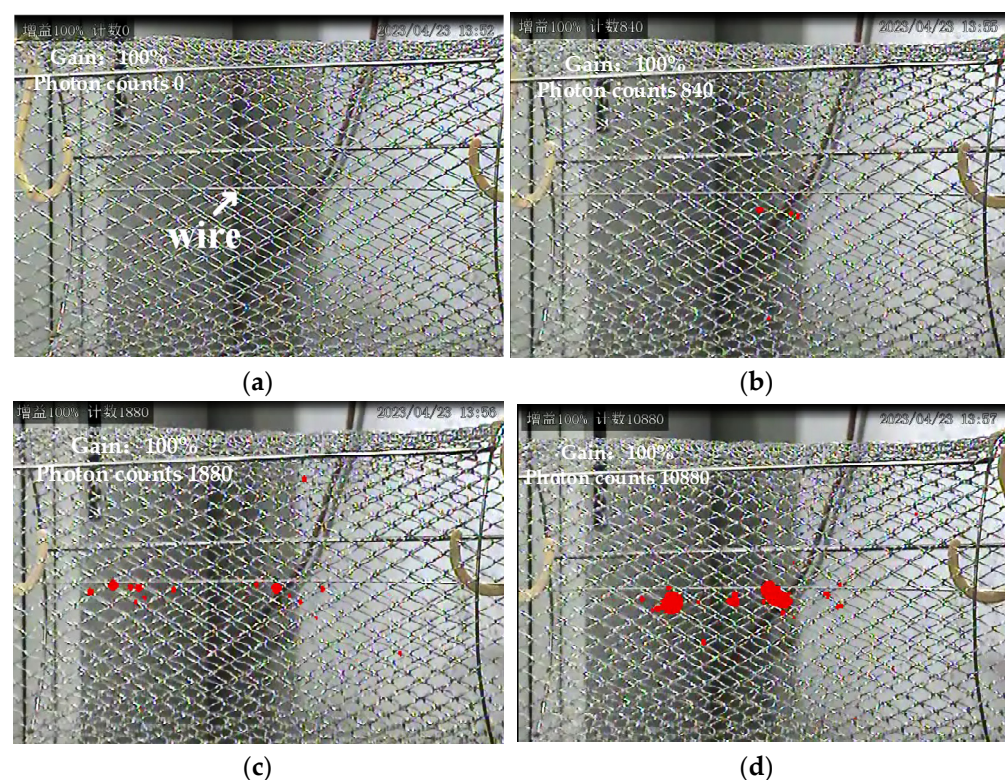


**Figure 3.** Typical ultraviolet images of 5 mm stainless-steel conductor at different voltages: (a) 50.0 kV; (b) 51.5 kV; (c) 52.5 kV; (d) 53.5 kV.

In Figure 3, the red dots represent clusters of photons measured using the ultraviolet imaging camera. Each spot represents a discharge point. From the figure, it can be observed that as the voltage increased, the area of the spots gradually increased, and they spread throughout the entire length of the conductor. This reflects the process of the conductor transitioning from no corona inception to full-scale corona inception. At low voltages, the corona discharge on the surface of the conductor may not be stable. The discharge points can intermittently ignite and extinguish, resulting in an intermittent presence of photons. As the voltage increased, the corona discharge on the surface of the conductor gradually became more stable. However, it still exhibited some intermittent behavior. The photon count shows systematic variations in response to this intermittent corona discharge. At higher voltages, the intensity of corona discharge on the surface of the conductor became more pronounced. The photon count increased rapidly as the voltage rose, and the area of the spots in the discharge image also increased. With the increase in voltage, the amplitude of the current also gradually increased. To gain a better visual understanding

of the relationship between the photon count and the corona current, the average photon number and corona current of a 5 mm conductor are plotted in Figure 4. When plotting the correlation diagrams of ultraviolet photon counts and current in this paper, the data in the figures represent the average measurements under constant parameters. Error bars were added to the curves in the images to reflect the fluctuation of the measurement results. The positive correlation between the photon count and the corona current indicates that the variation in the photon count accurately reflects the intensity of the discharge on the conductor. This suggests that changes in the photon count can provide a reliable indication of the discharge intensity of the conductor.

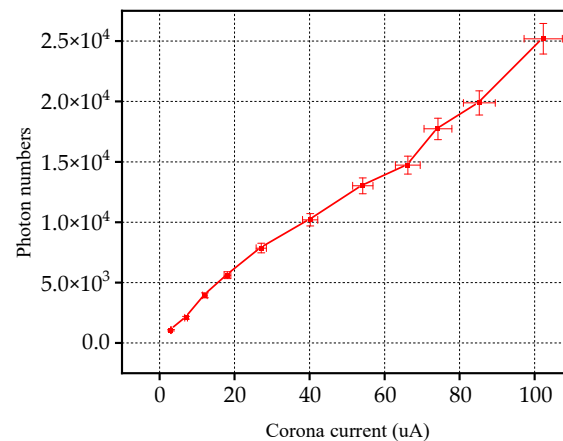


**Figure 4.** The relationship between photon count and corona current at different voltages.

From the above research, it can be observed that there was a positive correlation between the ultraviolet photon counts and the corona discharge current. Therefore, the discharge conditions of the conductor can be monitored using ultraviolet photon counts. In the laboratory, discharge experiments were conducted using a mini corona cage to perform corona discharge detection on three different specifications of smooth conductors under positive-polarity DC voltage. To observe weak corona discharge signals, the gain of the ultraviolet imaging camera was set to 100%, and the observation distance was set to 2 m. The relationships among the ultraviolet photon count, corona current, and voltage are studied, and the results are shown in Figure 5. From the figure, it can be observed that both the photon count and corona current increased with the increase in voltage. Additionally, the growth patterns of both variables appear to be similar or approximate. In the early stage of discharge, the photon count and corona current exhibited a slower increase with the voltage. As the voltage increased, the photon count and corona current showed a close-to-linear increase. However, once the voltage reached a certain level, the photon count and the corona current increased in an approximately exponential manner with the voltage.

The corona inception voltage of the conductor was determined using the inflection point method. The theoretical corona inception voltage calculated based on empirical equations and the corona inception voltage obtained through experimental measurements are presented in Table 2.

For the smooth conductor, the corona inception voltage obtained through measurements based on different corona discharge effects was generally consistent. From Table 2, it can be observed that the corona inception voltages obtained using three different methods for the smooth conductor had minimal differences. The maximum difference between the corona inception voltage obtained through the ultraviolet photon method and the empirical formula method was approximately 5%, while the maximum difference between the corona inception voltage obtained through the corona current method and the empirical formula method was approximately 7.5%. This indicates that the corona inception voltage obtained through the ultraviolet photon method was closer to the theoretical value. By using the

least squares fitting algorithm, the different conductor voltages and their corresponding ultraviolet photon counts can be fitted, resulting in a functional relationship, as shown in Table 3. In the table,  $U$  represents the voltage on the conductor, the unit is V, and  $n$  represents the ultraviolet photon count.

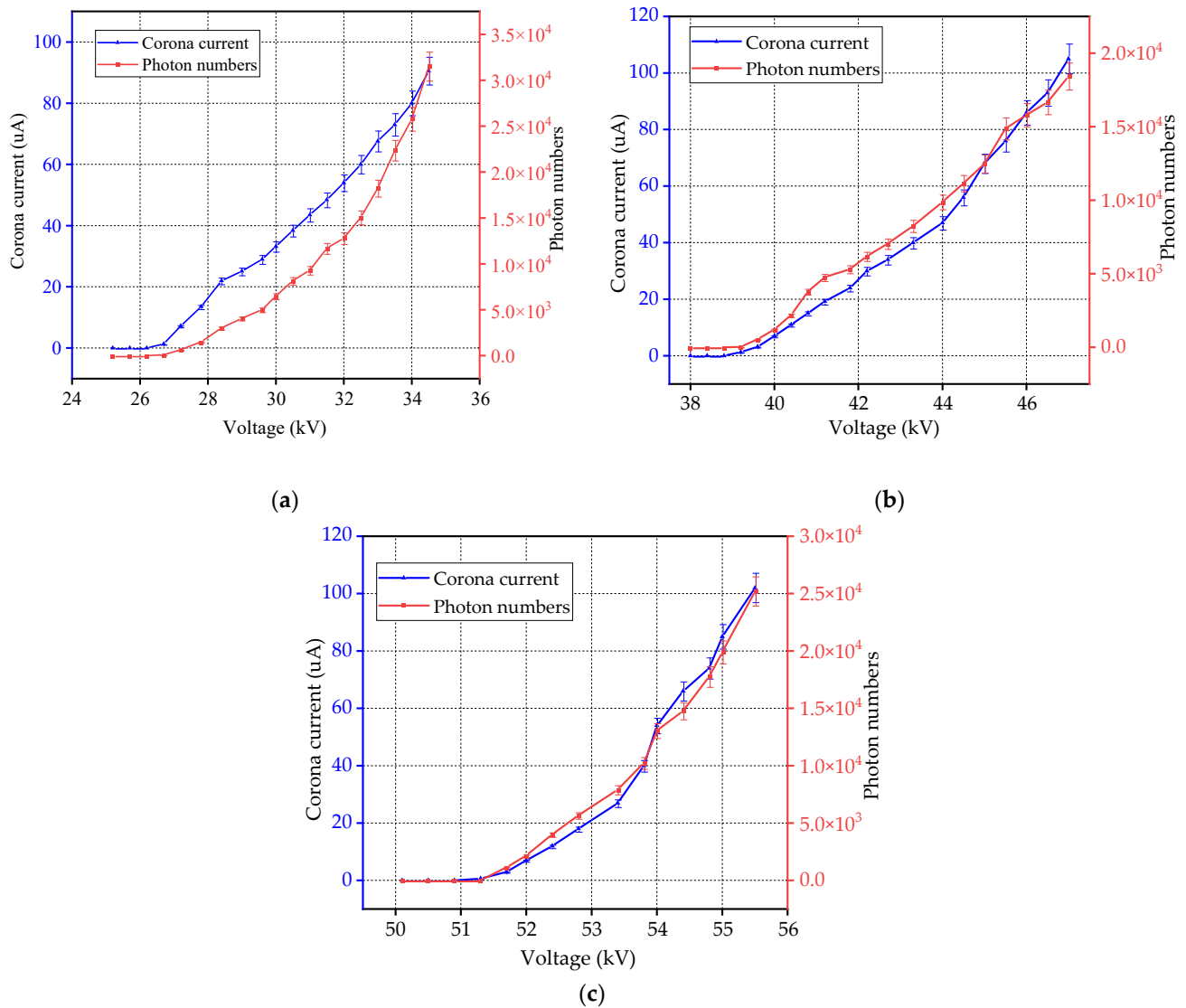


**Figure 5.** The relationships among the photon count, corona current, and voltage for conductors of different diameters. (a) 2 mm; (b) 3 mm; (c) 5 mm.

**Table 2.** The corona inception voltages of smooth conductors obtained using different research methods.

Research Method	Corona Voltage of 2 mm Diameter Conductor (kV)	Corona Voltage of 3 mm Diameter Conductor (kV)	Corona Voltage of 5 mm Diameter Conductor (kV)
Empirical formula method	28.99	38.22	51.77
Ultraviolet photon method	27.40	38.50	51.70
Corona current method	26.80	37.90	51.30

The calculation of the fitting coefficients shows that the fitted function has a coefficient of determination (R-squared) value greater than 0.99, which is close to 1. This indicates that the least squares fitting method provides a good fit for the relationship between the voltage and the ultraviolet photon count in relation to the three different specifications of conductors. From the fitting results, it can be observed that the relationship between the

ultraviolet photon count and the voltage follows a quadratic function, which is similar to the findings in reference [25].

**Table 3.** Expression of fitting function between UV photon number and voltage of conductors of different specifications.

Conductor Diameter (mm)	Fitting Function Expressions	Fit Coefficient
2	$U = -8.1525 \times 10^{-6} \times n^2 + 0.4856 \times n + 2.7028 \times 10^4$	0.9936
3	$U = -5.4202 \times 10^{-6} \times n^2 + 0.5222 \times n + 3.8204 \times 10^4$	0.9955
5	$U = -3.9799 \times 10^{-6} \times n^2 + 0.2592 \times n + 5.1455 \times 10^4$	0.9966

### 3.2. Characteristics of Photon Count with Gain and Observation Distance Variations

The experimental results indicate that the photon counts of the 2 mm, 3 mm, and 5 mm conductors have a consistent trend with the variations in the gain and observation distance of the ultraviolet imaging camera. Therefore, in this study, a conductor with a diameter of 5 mm was taken as an example to investigate the characteristics of photon count variations with changes in the gain and observation distance of the ultraviolet imaging camera. Figure 6 displays the ultraviolet photon count data obtained by varying the observation distance at different voltage levels while keeping the gain constant at 100%. An analysis of Figure 6 reveals that as the observation distance increased, the photon counts significantly decreased. When using ultraviolet detection to monitor corona discharge in electrical equipment, it is often considered that the discharge region of the equipment is much smaller compared to the detection distance. Therefore, the corona discharge source in the equipment being monitored is treated as a point source of light. As the detection distance increases, the energy emitted by the corona discharge source in the equipment gradually attenuates along the propagation path. Consequently, the photon counts obtained during detection decrease as the energy diminishes. These experimental results align with theoretical expectations.

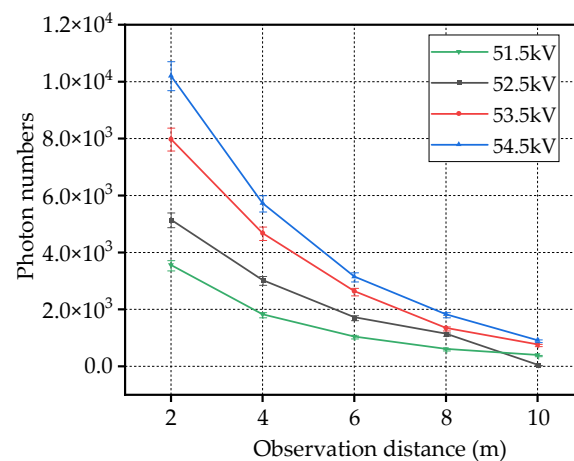


**Figure 6.** The relationship between the photon count and the observation distance.

By using the least squares method to fit the data points in Figure 6, the fitted function expression for the relationship between ultraviolet photon count and observation distance was obtained, and it is shown in Table 4. In the table,  $P$  represents the ultraviolet photon count, and  $L$  represents the observation distance in meters.

In Table 4, it can be observed that the fitted function expressions for photon count as a function of observation distance under different voltage levels have relatively high fitting coefficients. The relationship between the photon count and the observation distance follows an exponential function, with the exponent ranging from  $-0.2616$  to  $-0.2947$  and

with an average value of  $-0.2800$ . Thus, the relationship between the ultraviolet photon count and the observation distance under different voltages satisfies Equation (3).

$$P = ae^{bL} \tag{3}$$

**Table 4.** The fitted relationship expression between the ultraviolet photon count and the observation distance at different voltages.

Voltage (kV)	Fitting Function Expressions	Fit Coefficient
51.5	$P = 5857e^{-0.2769L}$	0.9891
52.5	$P = 8825e^{-0.2616L}$	0.9704
53.5	$P = 14322e^{-0.2867L}$	0.9786
54.5	$P = 18479e^{-0.2947L}$	0.9625

In the equation,  $P$  represents the ultraviolet photon count,  $L$  represents the detection distance, and  $a$  and  $b$  are constant coefficients. The value of coefficient  $a$  is related to the voltage magnitude (corona intensity) at the measured point, while coefficient  $b$  is set as the average of the exponent values from the fitted function expressions under different voltages in Table 4, which is  $-0.2800$ . Therefore, the ultraviolet photon count measured at different observation distances under a reference gain can be corrected to the ultraviolet photon count measured at a distance of 2 m. The specific process is as follows: for the same corona discharge light source, the relationship between the actual measured photon count  $P$  and the distance  $L$  is given by Equation (4):

$$P = ae^{-0.28L} \tag{4}$$

The relationship between the corrected photon count  $P_0$  and the distance  $L_0$  can be expressed as follows:

$$P_0 = ae^{-0.28L_0} \tag{5}$$

By combining Equations (4) and (5), we can obtain:

$$P_0 = Pe^{0.28(L-L_0)} \tag{6}$$

In the above equation,  $L$  is the actual observation distance,  $P$  is the photon count obtained from the actual observation,  $L_0$  is the reference distance, which is taken as 2 m in this paper, and  $P_0$  is the corrected photon count.

Based on Equation (6), the ultraviolet photon count measured at any detection distance can be corrected to the reference detection distance.

Using Equation (6) to correct the ultraviolet photon count to the reference detection distance, and then applying the fitted function relationship between the voltage and the ultraviolet photon count for the 5 mm conductor, we can determine the corresponding average ultraviolet photon count at the measured observation distance under the reference gain and the measurement distance, as well as the corresponding conductor voltage value, which provides a reference method for comparing the discharge intensity at different observation distances. By keeping the observation distance constant at 2 m and setting the gain of the ultraviolet detector within the range of 50 to 100, the variation in the ultraviolet photon count with respect to the gain at different voltages was obtained, as shown in Figure 7.

Analyzing Figure 7, the following characteristics of the photon count as a function of gain can be observed. With the increase in gain, the photon count did not monotonically increase or decrease. Instead, it underwent a process of initially increasing, then decreasing, and finally increasing again. When the instrument gain was low, with the increase in the instrument gain, some corona discharge signals that were not easily detectable at a low gain became measurable. The bright spots at the corona discharge locations gradually increased,

leading to a certain increase in the photon count. The corresponding gain ranged from 50% to 60%. However, when the instrument gain was set high and further increased, the discrete corona discharge spots on the screen were enlarged and merged with each other, forming a larger light spot. This affected the identification of the photon counts, resulting in a decrease in the photon count rather than an increase. The corresponding gain ranged from 60% to 80%. Therefore, from the experimental results, it can be seen that the detection performance was best when the gain was set to 60%.

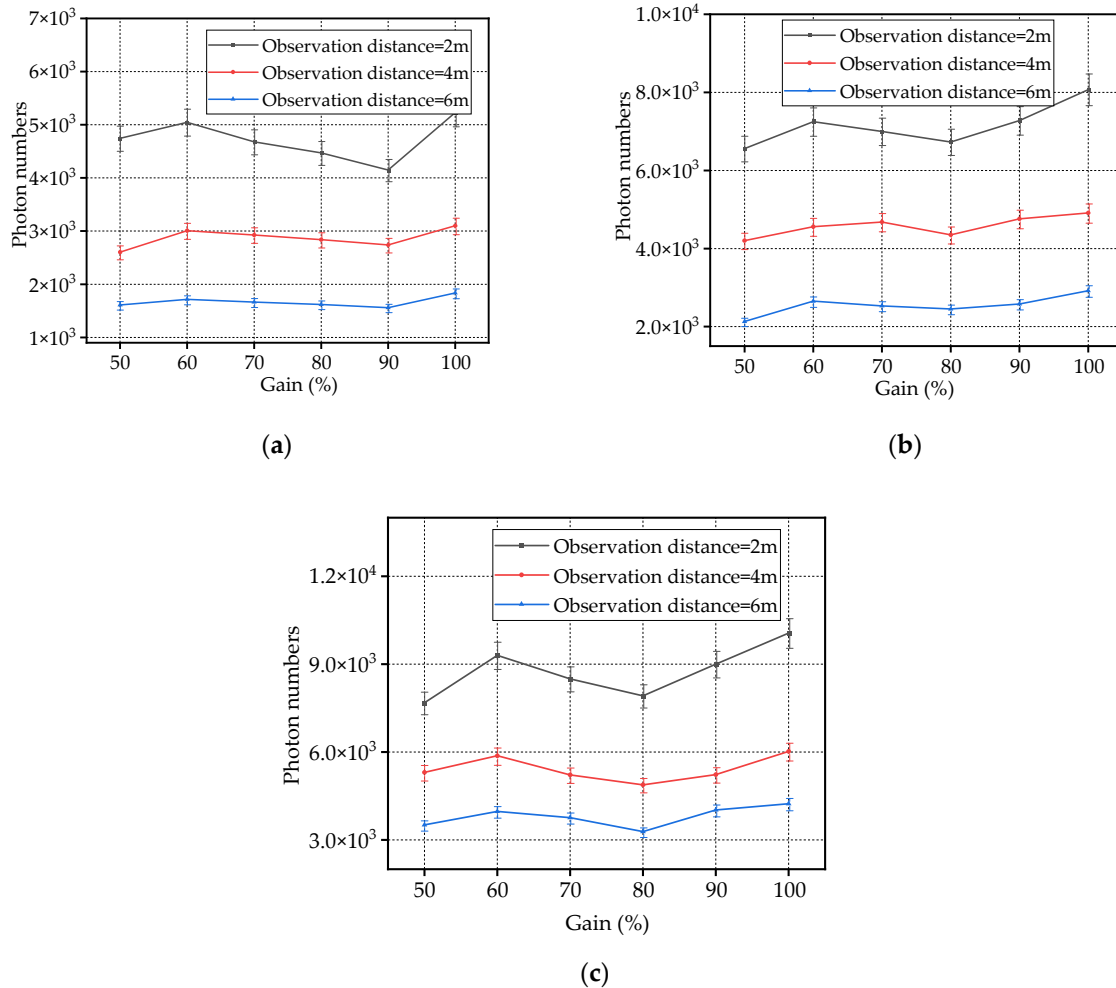


**Figure 7.** The variation in the photon count in relation to the gain under different applied voltages: (a) 52.5 kV; (b) 53.5 kV; (c) 54.5 kV.

## 4. Results and Analysis of Spot Area Detection

### 4.1. UV Detection Image Processing

The experimental results presented earlier indicate that the stronger the discharge intensity, the higher the photon count. The discharge point around the conductor appears as a spot in the ultraviolet image. Therefore, the area of the ultraviolet spot can be used to reflect the discharge intensity of the discharge location. As shown in Figure 8a, the ultraviolet detection images captured by the ultraviolet detector are RGB images. Their characteristic is that each pixel can be represented by three equally sized 2D arrays: R (red), G (green), and B (blue). To simplify the subsequent processing, the RGB image was converted into a grayscale image, as it contains more image information. Additionally, the k-means clustering algorithm was employed to segment the ultraviolet detection image. Unlike traditional image segmentation methods, the primary idea behind the k-means algorithm is to iteratively classify the data set into different clusters to achieve optimal

clustering capability [26]. Therefore, it is more suitable for segmenting ultraviolet detection images that are complex in shape and lack regularity.

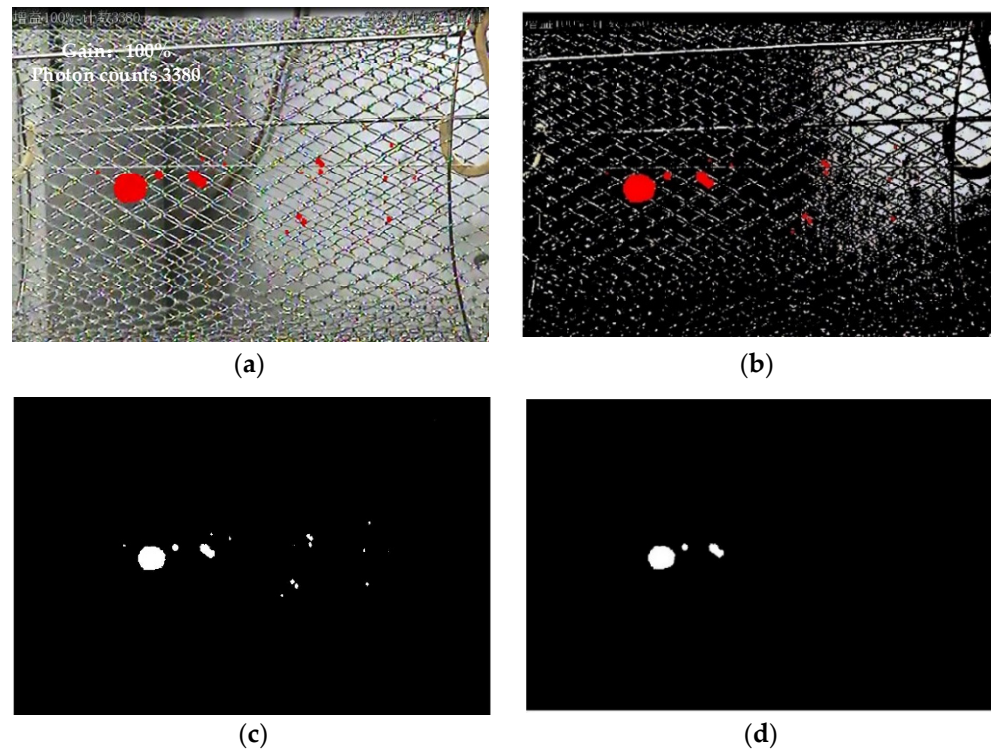


**Figure 8.** The image-processing process of ultraviolet detection images. (a) The original image; (b) grayscale processing; (c) image segmentation; (d) filtering.

In practical situations, when performing ultraviolet detection on power transmission lines, there are various challenges due to the complex field conditions and the presence of high-voltage electrical equipment. The ultraviolet images obtained from the ultraviolet imaging device are susceptible to interference, resulting in the presence of many noise points in the images. This interference can make it difficult for detection personnel to accurately determine the discharge locations on the power transmission lines. Therefore, this study employed mathematical morphological filtering algorithms to filter the ultraviolet detection images. The algorithm utilizes the opening operation to dilate the segmented ultraviolet image, eliminating discrete discharge points smaller than the structural element around the discharge area. It then applies the closing operation to fill in the cracks and concave regions outside of the discharge area, smoothing the discharge region [27]. The process of handling the ultraviolet detection image is illustrated in Figure 8.

#### 4.2. Calculation of Discharge Area Parameters in Ultraviolet Detection Images

After grayscale conversion, image segmentation, and filtering, clear discharge area contours with smooth and non-adhesive boundaries were obtained in the ultraviolet detection images. At this point, the area of the light spot in the ultraviolet detection image can be calculated using a function. In this study, the light spot area is defined as the number of white pixels in the image after spot recognition, measured in pixels. By applying Equation (7), the number of white pixels in the image can be counted to obtain the area of the corona discharge light spot. In the equation,  $M$  and  $N$  represent the rows and columns of the processed RGB image matrix, respectively.  $B(x, y)$  represents the number of white pixels, where  $x$  and  $y$  are the horizontal and vertical coordinates of the pixels in the processed matrix.

$$S = \sum_{i=1}^M \sum_{j=1}^N B(x, y) \quad (7)$$

Through the above process, the obtained images from the experiment were processed, and the following conclusions were drawn. For the 5 mm diameter conductor, when the gain of the UV imager was set to 100% and the observation distance was set to 2 m, the variation of the spot area with the voltage was observed. The relationship between the spot area and the voltage for the 5 mm conductor is depicted in Figure 9.

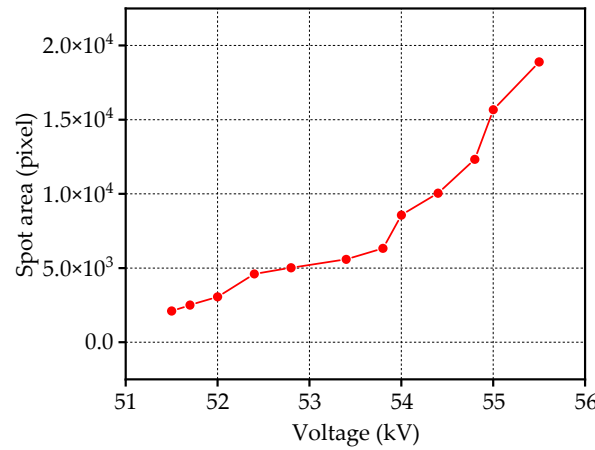


**Figure 9.** The relationship between the spot area and the voltage for a 5 mm diameter conductor.

The voltage and its corresponding UV spot area were fitted using the least squares fitting algorithm, and the obtained function relationship is shown in Equation (8). The calculated fitting coefficient for the function relationship is 0.9735, indicating a good fitting result. From the fitting results, it can be observed that the relationship between the spot area and the conductor voltage follows a quadratic function.

$$U = -1.5769 \times 10^{-8} \times S^2 + 5.5232 \times 10^{-4} \times S + 50.4771 \tag{8}$$

In the equation,  $U$  represents the applied voltage on the conductor, the unit is kV, and  $S$  represents the spot area.

**4.3. Characteristics of the Spot Area in Relation to Gain and Observation Distance Variations**

Figure 10 shows the variation of the spot area with changing observation distance while keeping the gain at 100%. Similar to the variation pattern of the UV photon count, the spot area decreased exponentially with increasing observation distance.

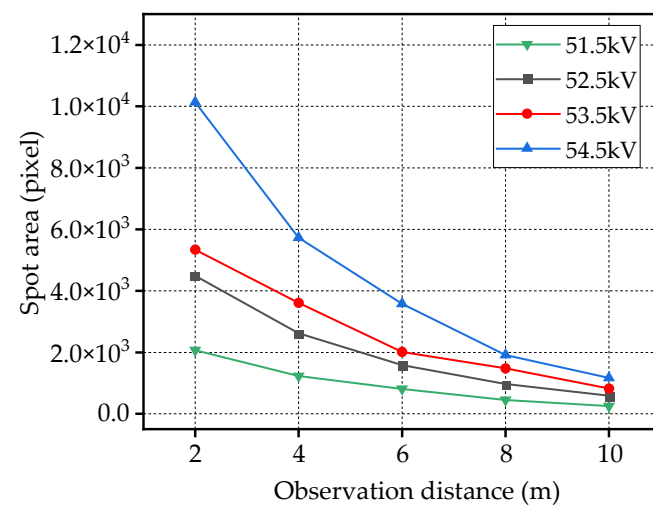


**Figure 10.** The variation trend of the discharge region area at different detection distances.

Using the least squares method, the data points in Figure 10 were fitted, and the fitted function expression for the spot area as a function of the observation distance is shown in Table 5. In the table,  $S$  represents the spot area in pixels, and  $L$  represents the observation distance in meters.

**Table 5.** The fitted relationship expression between the spot area and the observation distance at different voltages.

Voltage (kV)	Fitted Function Expression	Fit Coefficient
51.5	$S(L) = 3268e^{-0.2451L}$	0.9842
52.5	$S(L) = 7543e^{-0.2528L}$	0.9658
53.5	$S(L) = 8923e^{-0.2339L}$	0.9704
54.5	$S(L) = 17173e^{-0.2698L}$	0.9638

From Table 5, it can be observed that the fitted function expressions for the discharge area as a function of the observation distance have high fitting coefficients for each voltage level. The spot area exhibited an exponential relationship with the observation distance. Similarly to the process of Equations (3)~(6), we can obtain the correction of the spot area, with  $S$  at the actual observation distance to the spot area and  $S_0$  at the reference observation distance.

$$S_0 = Se^{0.2504(L-L_0)} \tag{9}$$

In the above equation,  $L$  is the actual observation distance,  $S$  is the spot area obtained from the actual observation,  $L_0$  is the reference distance in this paper, which is taken as 2 m in this paper, and  $S_0$  is the corrected spot area.

Keeping the observation distance constant at 2 m, and setting the gain of the UV detector between 50 and 100, the changed in the UV spot area with gain under different voltages could be observed, as shown in Figure 11.

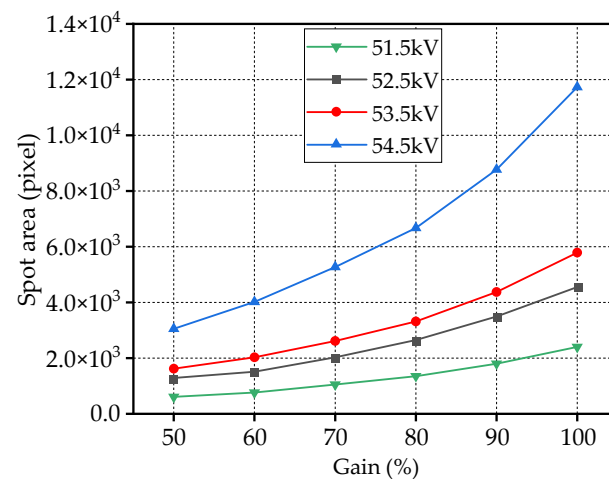


**Figure 11.** The variation of the discharge area with respect to the gain under different applied voltages.

Comparing Figures 7 and 11, it can be observed that under the same experimental conditions, the effects of gain on the photon count and spot area were different. The spot area shows a monotonous increase with the increase in the instrument gain. However, the photon count does not follow the same trend. When the gain increased from low to high, it did not monotonously increase with the gain. Instead, it exhibited a pattern of initial increase, followed by a decrease, and then an increase again. By observing the different characteristics of the photon count and spot area with respect to the instrument gain, it can be concluded that when the corona discharge is relatively stable, if the spot area is used as the reference factor for detection, the detection results will correspond directly to the instrument gain. If the photon count is used as the reference factor for detection, it is

possible to have similar detection results at different instrument gains. Therefore, more accurate results can be obtained by combining the two to detect discharge.

By using the least squares method to fit the data points in Figure 11, the fitting function expression for the relationship between the spot area ( $S$ ) and the gain ( $g$ ) was obtained and is shown in Table 6.

**Table 6.** Fitting relationship expression of discharge area with gain at different voltages.

Voltage (kV)	Fitted Function Expression	Fit Coefficient
51.5	$S(g) = 147.35e^{0.0279g}$	0.9571
52.5	$S(g) = 327.88e^{0.0263g}$	0.9353
53.5	$S(g) = 458.77e^{0.0250g}$	0.9737
54.5	$S(g) = 813.59e^{0.0267g}$	0.9631

From Table 6, it can be seen that the fitting coefficients of the function expressions for the photon count with respect to the observation distance are relatively high for each voltage level. The photon count is related to the observation distance in a power function relationship. Similarly to the process in Equations (3)~(6), the correction of the actual gain for the spot size to the reference gain can be obtained, as shown in Equation (10).

$$S_0 = S e^{0.0265(g_0 - g)} \tag{10}$$

In the above equation,  $g$  is the actual gain,  $S$  is the spot area obtained from the actual observation,  $g_0$  is the reference gain, which is taken as 100% in this paper, and  $S_0$  is the corrected spot area.

The formula to calibrate the spot size obtained at any detection distance and gain for a 5 mm conductor to the spot size at a gain of 100% and a detection distance of 2 m is as follows:

$$S_0 = S \cdot e^{0.0265(100 - g)} \cdot e^{0.2504(L - 2)} = S \cdot e^{2.1492 - 0.0265g + 0.2504L} \tag{11}$$

By combining Equations (8) and (11), the corresponding spot size at the reference detection distance and the reference gain for any detection distance and gain of the ultraviolet imaging device can be obtained, along with the corresponding voltage on the conductor. This allows for the evaluation of the discharge level of the conductor. To validate the correctness of this approach, using a UV imager, the UV photon count and spot area of a conductor with a diameter of 5 mm were measured at a detection distance of 7 m and a gain of 100. The voltage was then varied, and the measured UV photon counts and spot areas were obtained. These values were then corrected to obtain the reference photon counts and spot areas. The fitted voltage was determined by combining the reference photon counts and spot area with a voltage fitting function.

From Table 7, it can be seen that with the correction method and voltage fitting function proposed in this paper, accurate observations of corona discharge can be obtained. The error of the fitted voltage and the actual voltage was within 5%.

**Table 7.** UV imaging detection parameters and correction parameters under different voltages.

Discharge Area	Actual Photon Count	Corrected Photon Count	Actual Spot Area	Corrected Spot Area	Actual Voltage (kV)	Fitted Voltage (kV)
1	4903	19,882	3732	13,052	52.45	55.00
2	3193	12,948	2559	8949	51.65	54.10
3	1962	7956	1773	6201	51.84	53.30

## 5. Conclusions

This study conducted measurements and research on the photon count and spot area during corona discharge in relation to different sizes of smooth, stainless-steel conductors under positive DC voltage using a mini corona cage and further explored the variation patterns of the photon count and spot area during the corona discharge process. Additionally, this study analyzed the changes in photon count and spot area with respect to the UV imaging device gain and observation distance, and formulas were fitted to correct the actual measurement data to the reference measurement standard. The main conclusions are as follows:

- (1) The photon count and the spot area both exhibited a quadratic relationship with the conductor voltage, and they exhibited a close linear relationship with the corona current. Therefore, the ultraviolet photon count and the area of the light spot can be used to quantify the discharge intensity.
- (2) The photon count and spot area both decrease exponentially with an increasing observation distance. Under the conditions of ensuring a complete observation of the discharge area and maintaining a safe observation distance, the smaller the observation distance, the better the measurement results. The photon count exhibited a more complex relationship with the gain. As the gain increased, the photon count did not monotonically increase but underwent a process of initial increase, followed by a decrease, and then another increase. For the UV imager used in this study, the detection effect was best when the gain was 60%. On the other hand, the spot area showed an exponential increase with the gain. In practical engineering applications, the gain and observation distance can be adjusted according to the actual situation. Then, the calibration formula summarized in this paper can be used to correct the measurement parameters, which is convenient to compare the measured results under a unified standard and better evaluate the corona discharge intensity.
- (3) Both the photon count and the spot area can be used to describe the intensity of corona discharge. The photon count provides a more intuitive measure, while the spot area requires some image processing techniques. By using a combination of both UV detection parameters, it is possible to identify and characterize corona discharge phenomena in power transmission lines more accurately and comprehensively.

**Author Contributions:** Conceptualization, Y.D., Z.Z. and Z.D.; methodology, Z.Z., D.J. and Y.W.; software, Y.D.; validation, Y.D.; formal analysis, Y.D. and Z.Z.; investigation, Y.D.; resources, Y.W.; data curation, Y.D.; writing—original draft preparation, Y.D. and Z.Z.; writing—review and editing D.J., Z.D. and Y.W.; visualization, Y.D.; supervision, Z.Z. and Z.D.; project administration, Z.Z.; funding acquisition, D.J. All authors have read and agreed to the published version of the manuscript.

**Funding:** This work was supported by the National Natural Science Foundation of China (No. 52007011).

**Institutional Review Board Statement:** Not applicable.

**Informed Consent Statement:** Not applicable.

**Data Availability Statement:** The data that support the findings of this study are available from the corresponding author upon reasonable request.

**Conflicts of Interest:** Author Yongye Wu was employed by the company “Chengdu Power Supply Company”. The remaining authors declare that the research was conducted in the absence of any commercial or financial relationships that could be construed as a potential conflict of interest.

## References

1. Eifert, A.; Baier, T.; Hardt, S. Small Onset Voltages in Negative Corona Discharges Using the Edges of Gold and Aluminum Foils as Nano-Structured Electrodes. *Appl. Phys. Lett.* **2013**, *103*, 023114. [[CrossRef](#)]
2. Li, X.; Cui, X.; Lu, T.; Wang, D.; Peng, R.; Bian, X. Experimental Investigation on Correlation of Corona-Induced Vibration and Audible Noise from DC Conductor. *High Volt.* **2016**, *1*, 115–121. [[CrossRef](#)]

3. XingMing, B.; JunYu, Z.; Wei, Y.; ShuWei, W.; Lei, Q.; XueBao, L.; HaiBing, L. The Role of Low Air Pressure in the Variation of Negative Corona-generated Space Charge in a Rod to Plane Electrode. *High Volt.* **2018**, *3*, 126–132. [[CrossRef](#)]
4. He, Z.; Zhu, J.; Zhu, J.; Bian, X.; Shen, B. Experiments and Analysis of Corona Inception Voltage under Combined AC-DC Voltages at Various Air Pressure and Humidity in Rod to Plane Electrodes. *CSEE J. Power Energy Syst.* **2021**, *7*, 875–888. [[CrossRef](#)]
5. Wang, S.; Li, W.; Jiang, T.; Niu, L.; Lv, F.; Li, N. Study on the Influence Factors of Rod Plate Gap Corona Discharge Environment Based on UV Imaging. *IEEJ Trans. Electr. Electron. Eng.* **2021**, *16*, 35–43. [[CrossRef](#)]
6. Wang, Y.; Qian, Y. Evaluation Method for the Corona Discharge of Insulator Based on Convolution Neural Network with the Dual-Spectra Camera. *Opt. Eng.* **2020**, *59*, 103105. [[CrossRef](#)]
7. Lü, F.; Niu, L.; Wang, S.; Jiang, T.; Li, W.; Guo, J.; Li, H. Influencing of Water Droplets on Corona Inception Characteristics of Composite Insulator Recorded by UV Imager. *IET Sci. Meas. Technol.* **2020**, *14*, 1049–1056. [[CrossRef](#)]
8. Yin, K.; An, Y.; Hu, Y.; Qu, L.; Liu, X.; Lin, Y.; Su, M.; Yang, M.; Wang, Q.; Sha, X. Experimental Study on Positive Corona Discharge Characteristics in Plane-Single/Double Earthed Rods Air Gaps under Negative DC Voltage. *Electr. Power Syst. Res.* **2023**, *216*, 109058. [[CrossRef](#)]
9. Bian, X.M.; Wan, S.W.; Liu, L.; Wang, Y.J.; Macalpine, J.M.K.; Chen, L.; Wang, L.M.; Guan, Z.C. The Role of Charged Particles in the Positive Corona-Generated Photon Count in a Rod to Plane Air Gap. *Appl. Phys. Lett.* **2013**, *103*, 094102. [[CrossRef](#)]
10. Chongqing University; Mississippi State University; Southwest Jiaotong University (China); IEEE Dielectrics and Electrical Insulation Society; National Natural Science Foundation of China (China); Chinese Society of Electrical Engineering (Beijing, China); China Electrotechnical Society; Institute of Electrical and Electronics Engineers. In Proceedings of the ICHVE 2016: 2016 IEEE International Conference on High Voltage Engineering and Application, Chengdu, China, 19–22 September 2016; ISBN 9781509004966.
11. He, G.; Hu, Q.; Wu, B.; Shu, L.; Jiang, X.; Xiao, L.; Yu, Z. Influence of Freezing Water Conductivity on the Positive Corona Performance of Soft Rime Ice-Covered Conductor. *Int. J. Electr. Power Energy Syst.* **2019**, *112*, 137–143. [[CrossRef](#)]
12. Chen, L.; Bian, X.; Wang, L.; Guan, Z. Effect of Rain Drops on Corona Discharge in Alternating Current Transmission Lines with a Corona Cage. *Jpn. J. Appl. Phys.* **2012**, *51*, 09MG02. [[CrossRef](#)]
13. Bian, X.; Wang, L.; Liu, Y.; Yang, Y.; Guan, Z. High Altitude Effect on Corona Inception Voltages of DC Power Transmission Conductors Based on the Mobile Corona Cage. *IEEE Trans. Power Deliv.* **2013**, *28*, 1971–1973. [[CrossRef](#)]
14. Pinnangudi, B.; Gorur, R.S.; Kroese, A.J. Quantification of Corona Discharges on Nonceramic Insulators. *IEEE Trans. Dielectr. Electr. Insul.* **2005**, *12*, 513–523. [[CrossRef](#)]
15. Wang, S.; Lv, F.; Liu, Y. Estimation of Discharge Magnitude of Composite Insulator Surface Corona Discharge Based on Ultraviolet Imaging Method. *IEEE Trans. Dielectr. Electr. Insul. A Publ. IEEE Dielectr. Electr. Insul. Soc.* **2014**, *21*, 1697–1704. [[CrossRef](#)]
16. Zhang, Z.; Zhang, W.; Zhang, D.; Xiao, Y.; Deng, J.; Xia, G. Comparison of Different Characteristic Parameters Acquired by UV Imager in Detecting Corona Discharge. *IEEE Trans. Dielectr. Electr. Insul.* **2016**, *23*, 1597–1604. [[CrossRef](#)]
17. Li, Z.; Li, L.; Jiang, X.; Hu, J.; Zhang, Z.; Zhang, W. Effects of Different Factors on Electrical Equipment UV Corona Discharge Detection. *Energies* **2016**, *9*, 369. [[CrossRef](#)]
18. Lan, L.; Chen, X.; Wen, X.; Li, W.; Xiao, G. Calibration of Excitation Function Measurement Based on Corona Cage Test Results. *Rev. Sci. Instrum.* **2016**, *87*, 114704. [[CrossRef](#)] [[PubMed](#)]
19. Liao, R.; Liu, K.; Liu, H.; Wu, F. Measurement of Space Charge in Negative Corona on a Small Corona Cage. *IEEE Trans. Dielectr. Electr. Insul.* **2016**, *23*, 2344–2352. [[CrossRef](#)]
20. Yin, H.; Zhang, B.; He, J.; Wang, W. Measurement of Positive Direct Current Corona Pulse in Coaxial Wire-Cylinder Gap. *Phys. Plasmas* **2014**, *21*, 032116. [[CrossRef](#)]
21. Megala, V.; Karpagam, R.; Sathishkumar, G.K.; Gopinath, B.; Marish Kumar, P.; Deva Brindha, M. Investigation on Corona Performance of Conductors Using Fabricated Indoor Corona Cage. *Proc. Mater. Today Proc.* **2021**, *44*, 3652–3656. [[CrossRef](#)]
22. Urban, R.G.; Reader, H.C.; Holtzhausen, J.P. Small Corona Cage for Wideband HVac Radio Noise Studies: Rationale and Critical Design. *IEEE Trans. Power Deliv.* **2008**, *23*, 1150–1157. [[CrossRef](#)]
23. Zhang, Z.; Deng, B.; Deng, J.; Dai, Y.; Zhao, H.; Dong, Z. Microscopic Analysis of Trichel's Pulse Characteristics and the Effect of Air Pressure and Temperature. *Phys. Plasmas* **2022**, *29*, 123902. [[CrossRef](#)]
24. Liu, Y.P.; Zhu, L.; Lv, F.C.; Xie, X. Negative Corona Onset Characteristic of the UHV Conductors Based on the Corona Cage. *J. Electr. Eng. Technol.* **2014**, *9*, 2089–2097. [[CrossRef](#)]
25. IEEE Dielectrics and Electrical Insulation Society. Annual IEEE Computer Conference. In Proceedings of the IEEE Conference on Electrical Insulation and Dielectric Phenomena (CEIDP), Shenzhen, China, 20–23 October 2013; ISBN 9781479925971.
26. Qian, W.; Zhang, Y.; Chen, Y. Structures of Spurious Local Minima in K-Means. *IEEE Trans. Inf. Theory* **2022**, *68*, 395–422. [[CrossRef](#)]
27. Godse, R.; Bhat, S. Real-Time Digital Filtering Algorithm for Elimination of the Decaying DC Component Using Mathematical Morphology. *IET Gener. Transm. Distrib.* **2019**, *13*, 3230–3239. [[CrossRef](#)]

**Disclaimer/Publisher's Note:** The statements, opinions and data contained in all publications are solely those of the individual author(s) and contributor(s) and not of MDPI and/or the editor(s). MDPI and/or the editor(s) disclaim responsibility for any injury to people or property resulting from any ideas, methods, instructions or products referred to in the content.